Vibrational Spectroscopic Study on the Molecular Deformation Mechanism of a Poly(*trans*-1,4-diethyl muconate) Single Crystal Subjected to Tensile Stress

Shinsuke Nakamoto,[†] Kohji Tashiro,*[,†] and Akikazu Matsumoto[‡]

Department of Macromolecular Science, Graduate School of Science, Osaka University, Toyonaka, Osaka 560-0043, Japan; and Department of Applied Chemistry, Faculty of Engineering, Osaka City University, Sugimoto, Osaka 558-8585, Japan

Received July 12, 2002

ABSTRACT: A giant single crystal of poly(*trans*-1,4-diethyl muconate), obtained from the single crystal of the corresponding monomer by photoinduced solid-state polymerization reaction, was put under tension along the chain axis and the infrared and Raman spectra were measured as a function of tensile stress. The bands of skeletal vibrational modes were found to shift toward lower frequency side with relatively large amount, while those of side group did not shift very much or shifted rather to higher frequency direction. These data were analyzed on the basis of normal-modes calculation under a quasi-harmonic approximation, allowing us to estimate the microscopic deformation mechanism of the polymer chain under tension. The Young's modulus along the chain direction was calculated to be 63.8 GPa at 0 K, corresponding relatively well to the experimental value 47.1 GPa obtained from the stress−strain curve measured for the polymer single crystal at room temperature.

Introduction

When we try to understand the mechanical behavior of crystalline polymers from the structural point of view, we always encounter various serious problems, in particular the problem on heterogeneous stress distribution in the bulk sample, which may come from the complicated aggregation structure of crystalline and amorphous regions.[1−3] This complexity makes it difficult to discuss the deformation mechanism of polymer chain in the crystalline state from the atomistic level.[4] One of the most effective methods to avoid this difficulty may be to prepare a polymer single crystal of homogeneous morphology by utilizing a solid-state polymerization reaction of the corresponding monomer under an irradiation of γ-ray, for example.

Polymer single crystal is useful in such a point that the homogeneous stress distribution can be attained even for the bulk sample, as pointed out above. Another merit is that these single crystals may give us important information on the limiting mechanical property of the bulk samples. For most of the partially crystalline polymers the Young's modulus of the crystalline region has been estimated mainly by an X-ray diffraction technique, in which the bulk sample is put under tension and the stress−strain curve is obtained from the shift of diffraction peaks.[5] In this experiment, the stress is assumed to distribute homogeneously both in the crystalline and amorphous regions. However, this assumption is not always reasonable.[1−3,6−9] Rather the measurement of stress−strain curve for a giant single crystal of polymer is more decisive and direct in estimation of the Young's modulus of the crystalline region. The similar situation can be seen in the infrared and Raman spectral measurements made for the stressed polymer materials. The shift of the vibrational frequency, which is caused by an application of stress, is not necessarily common to the samples with various degrees of crystallinity,[1,2] suggesting a possibility of heterogeneous stress distribution in the bulk samples. In this case, also, the utilization of a giant single crystal must be quite useful for the direct estimation of the frequency shift in the crystalline phase.

However, a giant single crystal of a polymer is not easy to prepare. In the early stages of polymer science in 1920−1930, a solid-state polymerization reaction was already discovered for trioxane.[10] Unfortunately the thus prepared polyoxymethylene sample was of a multicrystalline state and was not a perfect single crystal.[11,12] So far there have been only a few cases in which polymer single crystal with a size large enough for manual treatment could be obtained. One typical example is seen in polydiacetylene.[13] As for a giant single crystal of this polydiacetylene, the mechanical deformation was investigated in detail through vibrational spectroscopic measurements under tension.[13,14] The X-ray structure analysis was made successfully under an application of tensile stress,[15] and the changes in atomic position could be traced directly. The estimated changes in the internal coordinates such as bond length, bond angle, etc. were found to be in good agreement with the lattice dynamically predicted deformation mechanism of this polymer.[14]

Poly(*trans*-1,4-diethyl muconate) (polyEMU) is another giant single crystal of this type.[16−19] This polymer is produced also by a photoinduced solid-state polymerization

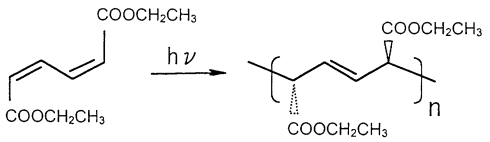

The structure change between monomer and polymer was clarified by the X-ray structure analysis: the space group symmetry is the same for both the monomer and

[†] Osaka University.
[‡] Osaka City University.

10.1021/ma021090q CCC: $25.00
Published on Web 01/07/2003

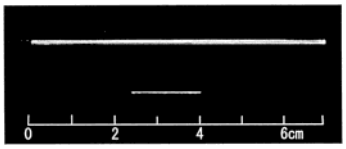

Figure 1. Photograph of polyEMU single crystals. The upper sample has a size of about 6.5 cm length, the largest single crystal obtained so far. The sample used actually in the present Raman experiment is the smaller one shown below.

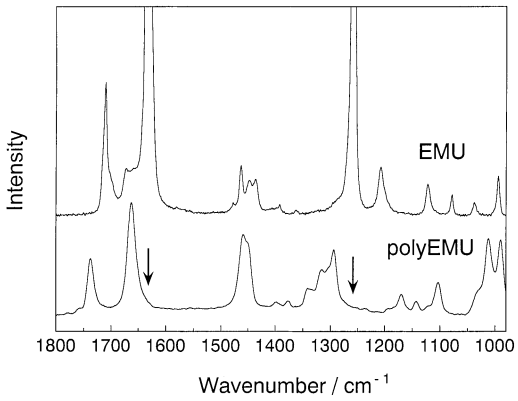

Figure 2. Raman spectra of EMU monomer and polyEMU.

polymer, indicating this reaction is a typical topotactic reaction.[20] Using the thus produced single crystal, we have measured the infrared and Raman spectra under application of tensile force along the chain axis. As described below, some of the bands were found to shift their position with increasing stress. These experimental data are interpreted in connection with the molecular deformation of the polymer chain. For this purpose, we have carried out the normal-modes analysis under quasi-harmonic approximation[21,22] and have been able to simulate the observed data semiquantitatively, from which the mechanism of molecular chain deformation is discussed.

As stated in the early part of this section, our purpose is to clarify the mechanical behavior of the bulk sample in relation with the stress distribution in the sample. PolyEMU is quite useful for this purpose because the semicrystalline samples with different morphology can be prepared easily by cooling the melt or by casting from the solution. The Raman spectra have been measured for these semicrystalline samples, which were found to show appreciably different behavior from that of the single crystal described in the present paper. By utilizing the experimental data obtained for the giant single crystal of polyEMU, the stress distribution in these semicrystalline samples may be deduced concretely and quantitatively. The details will be reported separately in the near future.

Experimental Section

Samples. Needlelike single crystals of EMU monomer were grown from the acetonitrile−water mixture solution in the dark room. These crystals were polymerized by ^{60}Co γ-ray irradiation (dosage 0.5 Mrad) at room temperature.[23] A photograph of the thus obtained polyEMU is shown in Figure 1. The average size was 1−2 cm in length, 1−2 mm in width, and 0.1−0.2 mm in thickness. Crystals with homogeneous cross-sectional area were carefully selected for the Raman measurement. The content of unreacted monomer component was checked by Raman spectra. For example, as seen in Figure 2, intense bands of monomer at 1633 and 1259 cm^{-1} were not observed in the spectra of polyEMU sample used in the present study, indicating that no monomer remained in the polymer single crystals.

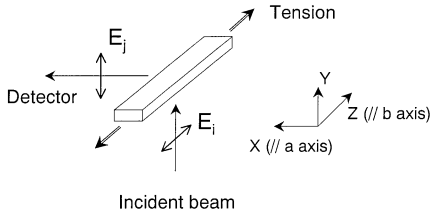

Figure 3. Illustration of scattering geometry to measure the polarized Raman spectra of polyEMU single crystal. $\mathbf{E}_i$ and $\mathbf{E}_j$ are the electric vectors of incident and scattered beams. In the case shown here, the (ZY) component can be measured.

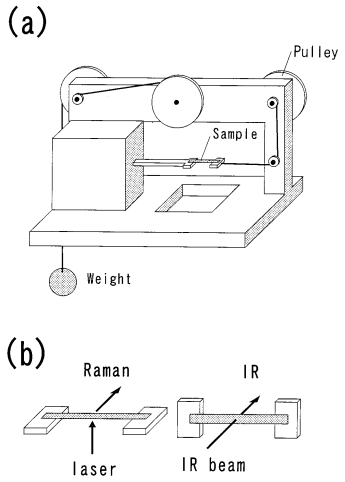

Figure 4. (a) Schematic diagram of an optical cell for Raman and infrared measurement under a constant stress. (b) Measurement modes of Raman and infrared signals.

Stress—Strain Curve. The stress−strain curve of polyEMU single crystal was measured in a manner similar to that described in ref 14. A single crystal was hang vertically and put under tension by applying a weight. The elongation of the sample was directly measured by a casettmeter.

Polarized Raman Spectral Measurements. To obtain useful information about the identification of the Raman bands, the polarized components of the Raman spectra were measured for the sample under tension free. The polarization component (ij) (i and $j = X$, Y, or Z) was recorded on the basis of the laboratorial coordinate system (X, Y, Z) defined in Figure 3, where the Z axis was parallel to the b axis (or the chain direction) and the X axis was parallel to the a axis. Figure 3 shows the scattering geometry used to measure the spectral component of (ZY), as an example. By changing the polarization direction of electric vector of incident and/or scattered light, the other spectral components were measured. For the (XX) and (YY) components, the sample was rotated to a suitable direction. Raman spectra were measured at a resolution power of 1 cm^{-1} by a Japan Spectroscopic Co. NR-1800 Raman spectrophotometer. A beam line with 514.5 nm wavelength from Ar$^+$ laser was used as an excitation light source.

Raman and Infrared Spectral Measurements under Tension. To measure the Raman and infrared spectra under tension, the sample was set into a stretcher as shown in Figure 4. Using this apparatus the sample deformation was made under a constant stress. By utilizing a set of pulleys, a small load gave a large force to the sample due to the principle of the lever. The sample was fixed on the metal holder at the both ends with screws and epoxy glue. The (ZZ) and (ZX) polarization components of the Raman spectra were measured. Infrared spectra were measured in a transmission mode for a platelet single crystal by using a Bio-Rad FTS-60A/896 FT-IR

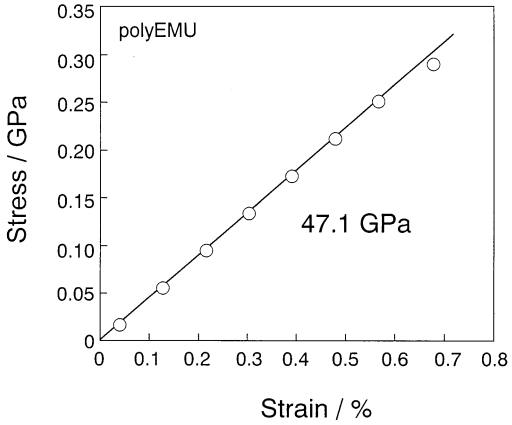

Figure 5. Stress−strain curve of polyEMU at room temperature.

Table 1. Correlation of Symmetry Species between the Molecular, Site, and Space Groups of PolyEMU

Molecular Group C_i	Site Group C_i	Space Group C_{2h}	Active Modes
Ag (XX, YY, ZZ, YZ, ZX, XY)	Ag	Ag	Raman (XX, YY, ZZ, XY)[a]
		Bg	Raman (YZ, ZX)
Au // ⊥	Au	Au	IR //[b]
		Bu	IR ⊥

[a] (*ij*) indicates the Raman polarizability component to be detected by irradiating a polarized incident light with electric vector $\mathbf{E}_i$ and detecting a scattered Raman signal with electric vector $\mathbf{E}_j$ (refer to Figure 3). [b] // and ⊥: polarization with an electric vector of incident infrared beam parallel and perpendicular to the chain axis (or the *b* axis), respectively.

spectrometer at a resolution power of 2 cm^{-1}. The sample was put under tension along the chain axis by the apparatus shown in Figure 4.

Results and Discussion

Stress—Strain Curve. Since the sample is a giant single crystal treatable by hands, we measured the stress−strain curve by applying a load directly to the sample and reading the sample length by a casettmeter. The stress−strain curve of a polyEMU single crystal is shown in Figure 5. A linear relation is seen between stress and strain in the strain region 0−1.0%, suggesting that polyEMU shows a Hookean elastic behavior. The Young's modulus along the chain axis was evaluated to be 47.1GPa from the slope. This value can be reproduced by lattice dynamical calculation, as will be mentioned in a later section.

Polarized Infrared and Raman Spectra of PolyEMU. The crystal structure of polyEMU was analyzed with X-ray diffraction methods as reported in the previous paper.[20] The PolyEMU chain in the crystal lattice possesses only points of symmetry and its factor group is isomorphous with the point group C_i. The factor-group vibrations of the chain are analyzed as

$$\Gamma = 41\ A_g\ (\text{Raman active}) + 39\ A_u\ (\text{IR active})$$

Symmetry correlation between the molecular group (C_i), the site group (C_i), and the space group (C_{2h}) is shown in Table 1. An A_g Raman-active mode of a single chain is predicted to split into two bands of A_g and B_g species with different polarization characters when the chains are packed into a unit cell. Similarly an infrared-active

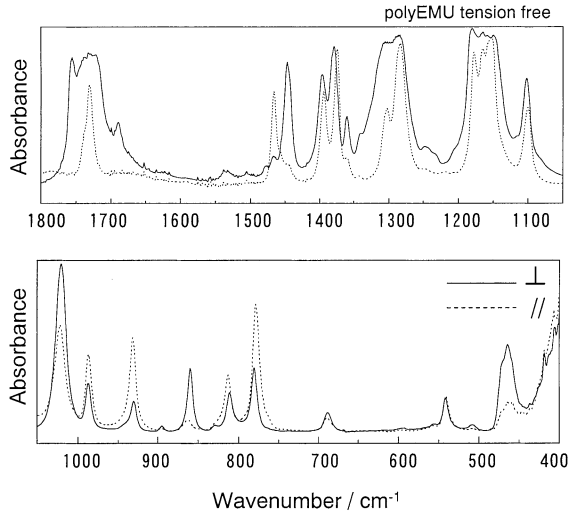

Figure 6. Polarized IR spectra of tension-free polyEMU single crystal. Solid and broken lines indicate the spectra taken with the electric vector of incident infrared beam perpendicular and parallel to the chain axis, respectively.

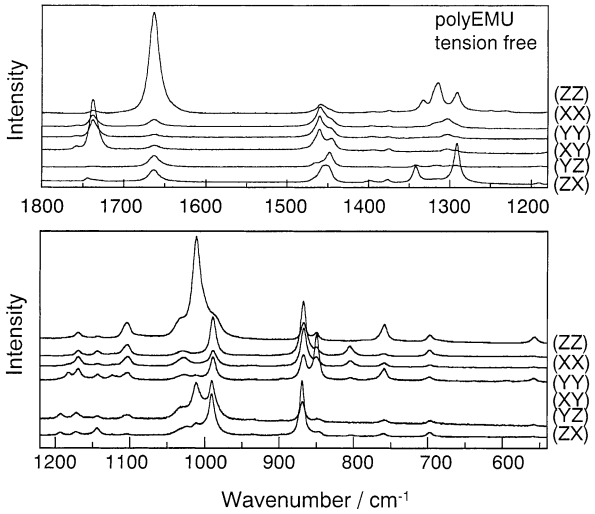

Figure 7. Polarized Raman spectra of tension-free polyEMU single crystal.

A_u mode splits into the A_u and B_u modes in the crystal lattice. A detailed discussion about the correlation splittings will be reported elsewhere. Polarized infrared spectra of polyEMU single crystal are shown in Figure 6. The solid and broken lines represent the spectra with the electric vector of the incident beam perpendicular and parallel to chain axis, respectively. Polarized Raman spectra in the frequency region 1800−500 cm^{-1} are shown in Figure 7. The bands with the polarizations (*ZZ*), (*XX*), (*YY*), and (*XY*) are assigned to the A_g modes, and those of (*YZ*) and (*ZX*) polarizations belong to the B_g species.

The normal-mode frequencies of a single chain were calculated on the basis of a *GF* matrix method, where the Urey−Bradley-type force field was employed for intramolecular interactions. This force field is convenient to introduce anharmonic effect into the force constants, as will be discussed in a later section. The force constants were quoted from those reported by Tadokoro et al.[24] and Shimanouchi et al.[25−27] with a slight modification and are listed in Table 2. The atomic coordinates obtained by X-ray structure analysis were used in the calculation.[20] Since the positions of hydrogen

Table 2. Harmonic and Anharmonic Force Constants of PolyEMU

	internal coordinate[a]	force constant[b] valence[c] harmonic	valence[c] anharmonic	repulsion[c] harmonic	repulsion[c] anharmonic
stretching	C_5═O_6	10.27	−1.00		
	C_1═C_2	7.70	−24.4		
	C_2−C_3	2.30	−1.00		
	C_3−C_4	2.21	−1.00		
	C_3−C_5	2.20	−1.00		
	C_5−O_7	3.50	−1.00		
	O_7−C_8	3.05	−1.00		
	C_8−C_9	4.10	−1.00		
	C_8−H	4.58	−1.00		
	C_9−H	4.30	−1.00		
	C_2−H_{10}	4.50	−1.00		
	C_3−H_{11}	4.26	−1.00		
bending	C_1═C_2−C_3	0.55	−0.57	0.54	−0.10
	C_2−C_3−C_4	0.55	−0.57	0.52	−0.10
	C_2−C_3−C_5	0.37	−0.40	0.52	−0.10
	C_4−C_3−C_5	0.37	−0.40	0.52	−0.10
	C_3−C_5═O_6	0.46	−0.40	0.65	−0.10
	C_3−C_5−O_7	0.56	−0.40	0.68	−0.10
	O_6═C_5−O_7	0.72	−0.40	1.35	−0.10
	C_5−O_7−C_8	1.58	−0.40	0.70	−0.10
	O_7−C_8−C_9	0.71	−0.40	0.75	−0.10
	C_1═C_2−H_{10}	0.27	+0.07	0.45	−0.10
	C_3−C_2−H_{10}	0.32	+0.07	0.40	−0.10
	C_5−C_3−H_{11}	0.44	+0.03	0.40	−0.10
	C_2−C_3−H_{11}	0.23	+0.05	0.30	−0.10
	C_4−C_3−H_{11}	0.33	+0.05	0.40	−0.10
	O_7−C_8−H	0.55	−0.20	0.365	−0.10
	C_9−C_8−H	0.55	−0.20	0.365	−0.10
	C_8−C_9−H	0.28	−0.20	0.250	−0.10
	H−C_8−H	0.23	−0.20	0.032	−0.10
	H−C_9−H	0.40	−0.20	0.032	−0.10
torsion	C'_4−C_1═C_2−C_3	0.15	−0.10		
	C_1═C_2−C_3−C_4	0.05	−0.10		
	C_2−C_3−C_4−C_1	0.05	−0.10		
	C_1═C_2−C_3−C_5	0.07	−0.10		
	C_5−C_3−C_4−C_1	0.07	−0.10		
	C_2−C_3−C_5−O_7	0.07	−0.10		
	C_3−C_5−O_7−C_8	0.28	−0.10		
	C_5−O_7−C_8−C_9	0.05	−0.10		
	C_4−C_3−C_5−O_7	0.07	−0.10		
out-of-plane	C_5═O_6	0.59	−0.10		
	C_2−H_{10}	0.31	−0.10		

[a] Definition of internal coordinates (refer to Figure 8). [b] Units of harmonic force constants: stretching and repulsion; mdyn/Å, and bending, torsion and out-of-plane; mdyn·Å/rad^2. Units of anharmonic force constants: stretching and repulsion; mdyn/Å^2, and bending, torsion and out-of-plane; mdyn·Å/rad^3. [c] Repulsion term is defined for a pair of end atoms of an anchor. For example, a repulsion between the atoms C_1 and C_3 is listed along with the bond angle or an anchor C_1−C_2−C_3.

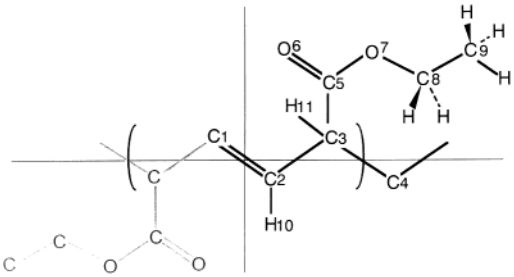

Figure 8. Numbering of constituent atoms of polyEMU used for the calculation of normal mode vibrations.

atoms were not so accurate as those of carbon and oxygen atoms, the hydrogen atom positions were calculated by using standard geometries. The numbering of the atoms is shown in Figure 8.

Observed and calculated vibrational frequencies of the Raman and infrared bands are listed in Tables 3 and 4 with the vibrational modes assignment, respectively. For both the infrared and Raman frequencies the calculated values are in good agreement with the observed data. In the process of band assignments, the deuterated polyEMU sample was used as well as the normal polyEMU sample. The details will be reported in a separate paper.

IR and Raman Spectral Changes under Tension. Stress dependence of the Raman spectra measured for the polyEMU single-crystal subjected to a tensile strain are reproduced in Figure 9 in the frequency regions 1650 and 1000 cm^{-1}. The band at 1663 cm^{-1}, which is assigned to the C═C stretching mode [ν(C═C)], is found to shift to the lower frequency side as the applied tension is increased. Similarly the two bands corresponding to the skeletal C−C symmetric stretching modes at 1033 and 1012 cm^{-1} also show the low-frequency shift. The stress dependence of IR spectra in the region of 1050−970 cm^{-1} are shown in Figure 10. The band of the skeletal C−C symmetric stretching mode at 1021 cm^{-1} was found to shift to lower frequency direction while the C−C stretching band of the side group at 985 cm^{-1} moved to higher frequency direction.

The stress dependence of the vibrational frequencies observed for the Raman and IR bands is plotted in Figure 11, parts a and b, respectively. The numerical

Table 3. Observed and Calculated Raman Frequencies (ν_0) and Shift Factor (α) of PolyEMU[a]

species	ν_0 (cm^{-1}) obsd	ν_0 (cm^{-1}) calcd[b]	α (cm^{-1}/GPa) obsd	α (cm^{-1}/GPa) calcd[b]	assignment[c]
A_g	3022	3007		−0.3	ν(=CH)
B_g					
A_g	2985	2978		0	ν_a(CH$_3$)
B_g	2990				
A_g	2985	2977		0	ν_a(CH$_3$)
B_g	2990				
A_g	2966	2958		0	ν_a(CH$_2$)
B_g	2968				
A_g	2942	2939		0	ν(CH)
B_g					
A_g	2903	2904		0	ν_s(CH$_2$)
B_g					
A_g	2879	2884		0	ν_s(CH$_3$)
B_g	2878				
A_g	1742	1739	0	0	ν(C=O)
B_g	1738				
A_g	1663	1663	−13.6	−13.8	ν(C=C)
B_g	1664				
A_g	1464	1472	0	0	δ(CH$_2$)
B_g	1452				
A_g	1464	1455		0	δ_a(CH$_3$)
B_g	1452				
A_g	1464	1449		0	δ_a(CH$_3$)
B_g	1452				
A_g	1397	1381	0	0	δ_s(CH$_3$)
B_g	1399				
A_g	1377	1345	0	0	w(CH$_2$)
B_g	1378				
A_g	1315	1318	0	−1.4	r(CH)
B_g	1316				
A_g	1303	1285	0	−0.1	t(CH$_2$) + r(CH$_2$)
B_g	1305				
A_g	1291	1296	−1.7	−2.9	ip(=CH)
B_g	1294				
A_g	1195	1205	0	−3.9	r(CH)
B_g					
A_g	1185	1161			ν(C$_3$C$_5$) − ν(C$_5$O$_7$) + ν(O$_7$C$_8$)
B_g	1186				
A_g	1170	1233	0	0	r(CH$_2$) + t(CH$_2$)
B_g	1173				
A_g	1145	1134	−1.4	−1.7	op(=CH) + ν(C$_3$C$_4$)
B_g	1146				
A_g	1103	1095	0	0	ν(C$_5$O$_7$) − ν(O$_7$C$_8$)
B_g	1104				
A_g	1033	1033	−3.5	−2.8	ν(C$_2$C$_3$)
B_g	1033				
A_g	1012	1013	−2.0	−2.7	ν(C$_3$C$_4$)
B_g	1012				
A_g	988	983	−0.4	−1.4	ν(C$_5$O$_7$) + ν(O$_7$C$_8$)
B_g	992				
A_g	933	924		0	ν(C$_3$C$_5$) + ν(C$_5$O$_7$)
B_g	936				
A_g	869	874	+1.2	−0.2	r(CH$_3$)
B_g	871				
A_g	851	851	−0.2	0	r(CH$_3$)
B_g	850				
A_g	759	785	0	−0.1	ip(C=O)
B_g	760				
A_g	699	687	−3.8	−0.2	op(C=O)
B_g	699				
A_g	560	554	−2.8	−2.6	δ(C$_1$=C$_2$C$_3$) + δ(C$_2$C$_3$C$_4$)
B_g	561				
A_g	466	471	−0.8	−1.0	δ(O$_7$C$_8$C$_9$)
B_g	461				
A_g	350	334	0	−0.1	δ(C$_5$O$_7$C$_8$) + ip(C$_5$=O$_6$)
B_g	347				
A_g	282	285	−0.6	−0.4	τ(C$_1$C$_2$C$_3$C$_4$) + τ(C$_5$C$_3$C$_4$C$_1$)
B_g	278				
A_g	220	230	−1.4	+0.2	δ(C$_2$C$_3$C$_5$)
B_g	222				
A_g	178	186		−0.6	δ(C$_5$C$_3$C$_4$)
B_g	185				
A_g	125	139		0	τ(C$_3$C$_5$O$_7$C$_8$)
B_g	134				
A_g	87	90		+0.1	τ(C$_2$C$_3$C$_5$O$_7$) + τ(C$_5$O$_7$C$_8$C$_9$) + τ(C$_5$C$_3$C$_4$C$_1$)
B_g	84				
A_g	49	50		0	τ(C$_5$O$_7$C$_8$C$_9$)
B_g	47				
A_g		36		0	τ(C$_4$C$_3$C$_5$O$_7$) + τ(C$_2$C$_3$C$_5$O$_7$) + τ(C$_3$C$_5$O$_7$C$_8$)
B_g					

[a] ν_0 is a vibrational frequency of tension-free polyEMU. The vibrational frequencies were measured for both of A_g and B_g species and the shift factor wasre only for the A_g bands. [b] Calculated for an isolated single chain. [c] The band splitting into A_g and B_g was not taken into account. [d] Key: ν, stretching; δ, bending; w, wagging; t, twisting; r, rocking; ip, in-plane mode; op, out-of-plane mode and τ, torsion. ν(=CH) is a stretching mode of C−H bond of ethylene unit. Subscripts "a" and "s" indicate antisymmetric and symmetric modes, respectively.

value indicated on the side of each band is the shift factor or the frequency shift per 1 GPa of tensile stress. In the observed Raman spectra, the bands related to the skeletal vibrations at 1663, 1033, 1012, and 560 cm^{-1} are found to show relatively large shift toward the lower frequency direction with increasing stress. The bands assigned to the vibration modes of the side groups did not shift as much as the skeletal vibrational modes. Similar tendency was also observed in the infrared spectra.

Quantitative Analysis of the Frequency Shift. The stress-induced frequency shift is considered to come mainly from the anharmonic effect of the potential field. To interpret the observed shift factors quantitatively, a quasi-harmonic approximation was introduced in the normal-mode calculation.[21,22] In this approximation the force constant F is assumed to be a linear function of such an internal displacement coordinate ΔR as bond stretching, bond angle deformation, etc.

$$F = F^\circ + F'\Delta R \tag{1}$$

where F° and F' are the harmonic and anharmonic terms of the force constant, respectively. When the molecular chain is put under tension along the chain axis, the internal coordinate such as bond length or bond angle is changed more or less. This change affects the force constant as seen in eq 1. Because the vibrational frequency ν is proportional to the square root of F, ν can be expressed in terms of ΔR or as a function of stress.[21,22]

In the actual calculation the anharmonic terms F' were determined by a trial-and error method so that the observed frequency shifts could be reproduced as well as possible. The calculated stress dependence of the Raman band frequency is compared with the observed data in Figure 12. The frequency shift factors α estimated for various vibrational modes are summarized in Tables 3 and 4. The observed frequency shift of the skeletal vibration modes is reproduced relatively well in the calculation. For some of the side group modes, the agreement between the observed and calculated results is not very good. This may be due to the neglect of the intermolecular interactions which may affect the vibrational frequencies of the side groups more or less.

The numerical values of harmonic and anharmonic force constants are listed in Table 2. The anharmonic force constant F' for double bond stretching mode ν[C=C] is quite large compared with those of C−C bonds. As discussed before,[4] the shape of potential energy curve V is determined by a combination of F° and F' as

$$V(\Delta R) \approx (^1/_2)F^\circ(\Delta R)^2 + (^1/_6)F'(\Delta R)^3 \tag{2}$$

Table 4. Observed and Calculated Infrared Frequencies (ν_0) and Shift Factor (α) of polyEMU[a]

species	ν_0 (cm^{-1}) obsd	ν_0 (cm^{-1}) calcd[b]	α (cm^{-1}/GPa) obsd	α (cm^{-1}/GPa) calcd[b]	assignment[c]
A_u	3006	3022		0	ν(=CH)
B_u	3008				
A_u	2982	2987		0	$\nu_a(CH_3)$
B_u	2985				
A_u	2982	2977		0	$\nu_a(CH_3)$
B_u	2985				
A_u	2962	2958		0	$\nu_a(CH_2)$
B_u	2964				
A_u	2941	2953		0	ν(CH)
B_u	2947				
A_u	2900	2904		0	$\nu_s(CH_2)$
B_u	2905				
A_u	2878	2884		0	$\nu_s(CH_3)$
B_u	2876				
A_u	1738	1739	0	0	ν(C=O)
B_u	1739		0		
A_u	1467	1472	0	0	$\delta(CH_2)$
B_u	1447		0		
A_u	1467	1455	0	0	$\delta_a(CH_3)$
B_u	1447		0		
A_u	1467	1449	0	0	$\delta_a(CH_3)$
B_u	1447		0		
A_u	1397	1381	0	0	$\delta_s(CH_3)$
B_u	1394		0		
A_u	1375	1345	0	0	$w(CH_2)$
B_u	1380		0		
A_u	1360	1354	−2.3	−2.2	ip(=CH)
B_u	1360		−2.5		
A_u	1303	1316		−0.7	r(CH)
B_u	1306				
A_u	1278	1285		0	$t(CH_2) + r(CH_2)$
B_u	1278				
A_u	1178	1195		−3.7	w(CH)
B_u	1180				
A_u	1165	1168		−0.5	$\nu(C_3C_5) - \nu(C_5O_7) + \nu(O_7C_8)$
B_u	1164				
A_u	1152	1233		0	$r(CH_2) + t(CH_2)$
B_u	1154				
A_u	1100	1099	+0.8	0	$\nu(C_8C_9) + \nu(O_7C_8)$
B_u	1104		−0.8		
A_u	1021	1025	−1.8	−2.0	$\nu(C_2C_3)$
B_u	1022		−1.5		
A_u	985	985	+1.5	−0.8	$\nu(C_2C_3) + \nu(O_7C_8) + \nu(C_8C_9)$
B_u	987		+2.0		
A_u	930	944	0	0	$\nu(C_5O_7)$ +op(=CH)
B_u	931		0		
A_u	895	888	0	−0.1	$\nu(C_5O_7) + \delta(C_5O_7C_8) + r(CH_3)$
B_u	897		0		
A_u	860	860	0	−0.1	op(=CH) +$\nu(O_7C_8)$
B_u	862		0		
A_u	812	850		0	$r(CH_3)$
B_u	813				
A_u	780	756	0	+0.3	ip(C=O)
B_u	779		0		
A_u	688	675	0	−0.2	op(C=O) + $\nu(C_3C_5)$
B_u	688		0		
A_u	542	541	−1.5	−1.3	$\delta(C_1{=}C_2C_3) + \delta(C_2C_3C_4)$
B_u	542		−1.8		
A_u	467	473		−1.1	$\delta(O_7C_8C_9)$
B_u	468				
A_u	361	345		−0.4	$\delta(C_5O_7C_8)$
B_u	381				
A_u	305	322		−0.4	$\tau(C_4C_1{=}C_2C_3) + \delta(C_2C_3C_4) + \delta(C_2C_3C_5)$
B_u	298				
A_u	268	264		−0.5	$\delta(C_3C_5O_7) + \delta(O_5O_7C_8) + \delta(C_1C_2C_3)$
B_u					
A_u	230	186		+0.4	$\tau(C_3C_5O_7C_8) + \delta(C_2C_3O_5)$
B_u	199				
A_u		98		0	$\tau(C_5O_7C_8C_9) + \tau(C_4C_3C_5O_7) + \tau(C_1C_2C_3C_5)$
B_u					
A_u		64		0	$\tau(C_5O_7C_8C_9) + \tau(C_4C_3C_5O_7)$
B_u					
A_u		45		0	$\tau(C_2C_3C_5O_7) + \tau(C_4C_3C_5O_7) + \tau(C_5C_3C_4C_1)$
B_u					
A_u		37		0	$\tau(C_5O_7C_8C_9) + \delta(C_1{=}C_2C_3)$
B_u					

[a] ν_0 is a vibrational frequency of tension-free polyEMU. [b] Calculated for an isolated single chain. The band splitting into *Au* and *Bu* was not taken into account. [c] Refer to the footnote in Table 3.

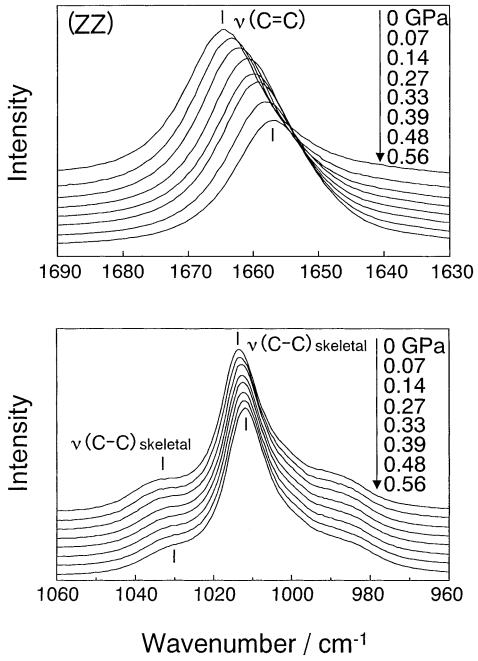

Figure 9. Stress dependence of the Raman (*ZZ*) spectra measured for skeletal C=C and C−C stretching bands of polyEMU.

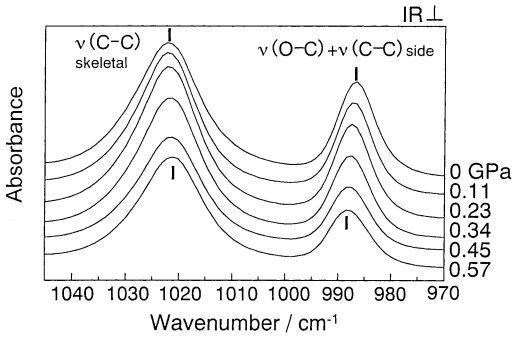

Figure 10. Stress dependence of the infrared spectra (perpendicular component) of polyEMU.

As shown in Figure 13, the potential energy curve of C=C stretching mode is highly asymmetric with respect to the origin of ΔR axis when an anharmonic term F' is introduced into the potential function, different from the case of C−C stretching mode. This can be seen as a general tendency and may be due to the characteristic feature of the molecular orbitals associating with the C=C double bond. Quantum mechanical interpretation of large frequency shift of strained polyEMU chain will be an important theme in future. It should be emphasized here that the shape of potential function, which is quite important in the prediction of structure and/or physical property of a material can be known experimentally on the basis of the observed stress dependence of vibrational frequencies.

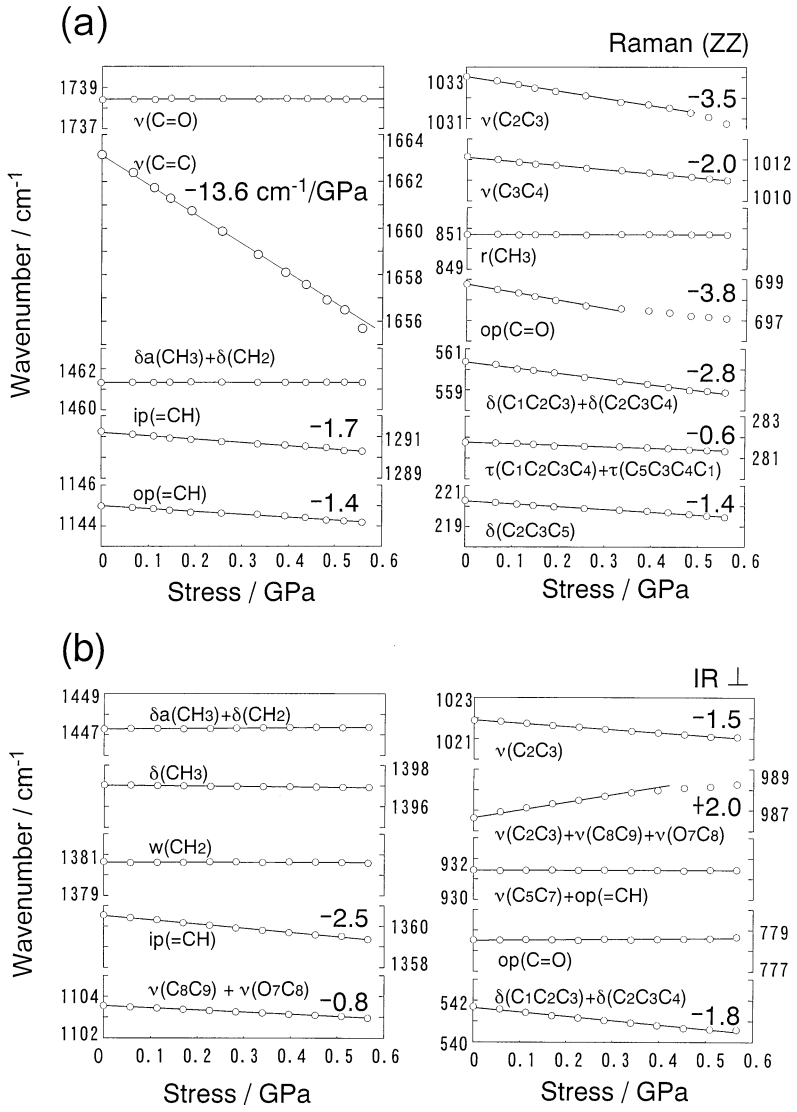

Figure 11. Stress dependence of vibrational frequencies evaluated for (a) Raman (*ZZ*) spectra and (b) infrared spectra (B_u mode) of polyEMU.

Molecular Deformation Mechanism and Frequency Shift Factor. The Young's modulus along the chain axis was calculated at the same time with the above-mentioned vibrational frequencies. The calculation method was described in detail in reference.[4] The calculated value is 63.8 GPa at 0 K. The modulus observed at room temperature is 47.1 GPa, a little lower than the calculated value, but it may be reasonable when the temperature effect is taken into account. As another factor we might need to consider the contribution of intermolecular interactions, although it generally increases the modulus.

Figure 14a shows the atomic displacements and potential energy distributions calculated for an isolated polyEMU chain subjected to a hypothetically large tensile strain of 10%. The potential energy distribution (PED) or the distribution of strain energy to internal coordinates is defined in the following equation.[4]

$$(\mathrm{PED})_i = F^\circ_{ii}(\Delta R_i)^2/\Sigma F^\circ_{ii}(\Delta R_i)^2 \times 100\ (\%)$$

where ΔR_i is the ith internal displacement coordinate and F°_{ii} is the diagonal element of the force constant matrix. As seen in this figure, when the chain is put under tension along the chain axis, the strain energy distributes mainly to the stretching of skeletal C−C and C═C bonds and the CCC bond angle deformation. This energy distribution corresponds well to the experimental result that only the vibrational modes of skeletal CC bond stretching and CCC bond angle deformation show remarkable frequency shifts. At the same time, however, we need to notice that the torsional angle of the skeletal chain is also changed in this mechanical deformation of the chain. The polyEMU skeleton takes a conformation of ...TS-trans-$\bar{S}$T... as shown below, and

$$\cdots\!-\!CH\!-\!CH\!=\!CH\!-\!CH\!-\!CH\!-\!\cdots$$
$$\mathrm{T\quad S\quad trans\quad \bar{S}\quad T}$$

the repeating period along the chain axis is contracted by ca. 0.16 Å from the all-trans zigzag conformation (from 5.00 to 4.84 Å). Because of this skew conformation, the chain deformation occurs through the torsional angle change as well as the changes in bond lengths and bond angles. In fact a Raman band at 282 cm^{-1} was found to show relatively large frequency shift by tension, which was assigned to the skeletal torsional mode as shown in Table 3. The relatively low Young's modulus of this polymer chain is considered to come from such a molecular deformation mechanism shown in Figure 14

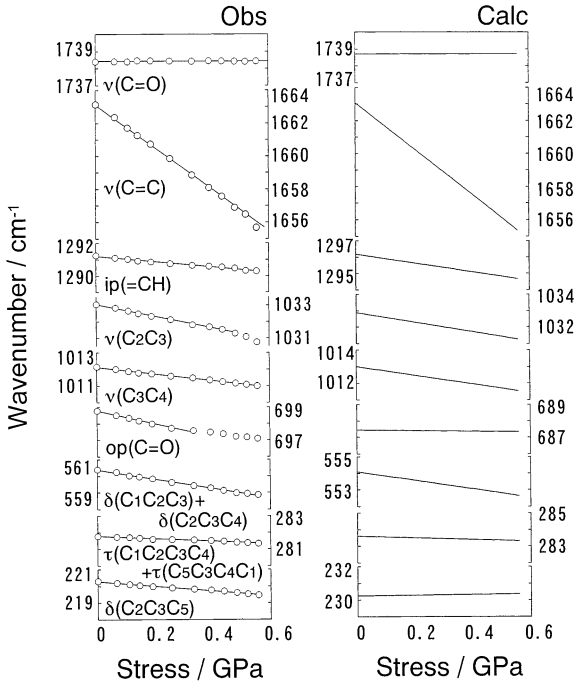

Figure 12. Comparison between the observed and calculated vibrational frequency shifts of various Raman bands of polyEMU.

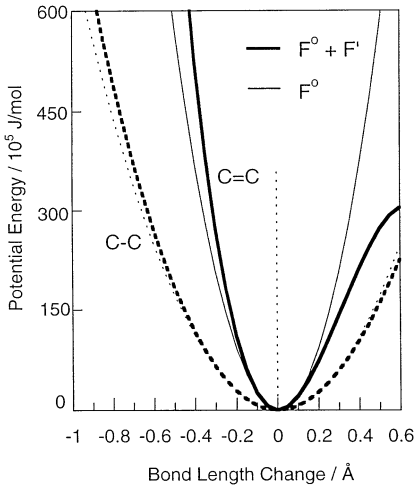

Figure 13. Potential energy functions calculated for C═C and C−C bond stretching modes of polyEMU using the harmonic ($F°$) and anharmonic (F') force constants shown in Table 2 (refer to eq 2). Bold lines: with $F°$ and F' taken into account. Thin lines: only with $F°$ taken into account.

(a). We know several polymers which have similar skeletal conformations with polyEMU. For example, poly(*trans*-1,4-butadiene)[28] and poly(*trans*-1,4-isoprene)[29] take the molecular conformation of trans-STS, quite similar to that of polyEMU. Although the crystallite modulus or the Young's modulus in the crystalline region has not yet been measured for these two polymers, we estimated it theoretically. The Young's modulus along the chain axis is 170.8 GPa for poly(*trans*-1,4-butadiene), which was calculated by using a geometry reported in ref 28 and the force constants listed in Table 2. The Young's modulus of poly(*trans*-1,4-butadiene) is apparently 3 times higher than that of polyEMU. Because the effective cross-sectional area of a single chain is different, the so-called extensibility Φ or the force necessary for stretching the molecular chain by 1% was calculated. The result is shown in Table 5. Φ is

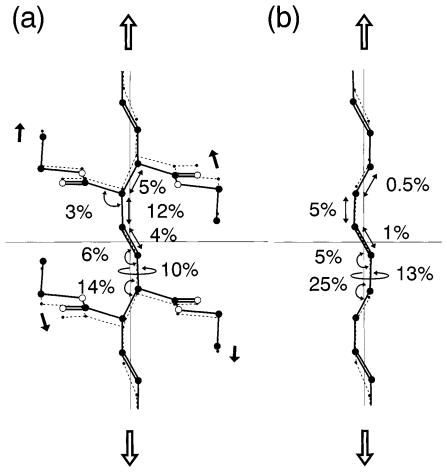

Figure 14. Atomic displacements and potential energy distributions calculated for (a) polyEMU and (b) poly(*trans*-1,4-butadiene) single chains under a tensile strain of 10%. The broken line represents the structures subjected to a tension.

Table 5. Comparison of Mechanical Property of Two Butadiene Polymers

	Young's modulus (calcd) (GPa)	cross-sectional area (Å^2)	extensibility, Φ (N)
polyEMU	63.8	54.5	3.48×10^{-10}
poly(*trans*-1,4-butadiene)	170.8	18.0	3.07×10^{-10}

essentially the same between these two polymers, supporting a similar deformation mechanism of the chain. In fact, as seen in Figure 14, parts a and b, the potential energy distribution is similar to each other, reflecting a similarity in molecular chain conformation. A slight difference in PED may come from the slight difference in molecular geometry parameters between them.

We need now to know the relationship between the above-mentioned deformation mechanism and the stress-induced frequency shifts. As already discussed in a previous paper,[4] the frequency shift $\Delta\nu$ is approximately expressed by the following equation

$$\Delta\nu \propto BF'(\mathrm{PED})^{1/2}/F° \qquad (4)$$

where B is a component of the **B** matrix and is determined by the geometry of the chain. This equation indicates that a larger shift of vibrational frequency is predicted for the vibrational mode of the internal coordinate with softer chemical bond (smaller $F°$) and higher anharmonicity (larger F'). Besides the internal coordinate to which the strain energy (or PED) is preferentially distributed should show higher frequency shift. As seen in Figure 14, the PED is concentrated on the bond stretching, bond angle deformation, and torsional angle deformation of the skeletal chain, corresponding well to the large frequency shift factors observed for the skeletal vibrational modes.

Conclusions

In the present paper, the infrared and Raman spectra were measured for polyEMU single crystal subjected to tensile stress, and a large frequency shift was found for the vibrational bands related with the skeletal chain part. This experimental data could be interpreted reasonably by carrying out the normal modes calculation with the anharmonic force constants taken into

consideration. This calculation gave us useful information on the microscopically viewed deformation mechanism of this polymer chain. Among the many internal coordinates, only the coordinates related with the skeletal chain were found to owe the deformation of the chain as understood from larger shift in vibrational frequency and higher distribution of strain energy to the corresponding internal coordinates. In particular, the energy distribution to the torsional angles around the skew-type skeletal bonds cannot be neglected in addition to the distribution to the skeletal CC bond stretching and CCC bond angle deformation. This deformation mechanism was related with the relatively low Young's modulus along the chain axis. The similarity in mechanical behavior was also discussed between polyEMU and poly(*trans*-1,4-butadiene) with similar chain conformation. The information on harmonic and anharmonic force constants obtained in this experiment allowed us to evaluate the shape of potential energy functions.

In this paper, we discussed the mechanical behavior of single crystal of polyEMU. The experimental data obtained here may be assumed as limiting values for this synthetic polymer. Fortunately we can control the morphology of this polymer by melting the sample and cooling it down to various temperatures or by casting from the solution. The mechanical behavior of these samples with different morphology is predicted to be quite different from that of the single crystalline state. That is to say, through the comparison of the spectroscopic data collected for these various samples under tension, we may clarify the difference in mechanical behavior or the difference in stress distribution due to the morphological difference because we have known now the behavior of pure crystalline state. Some experiments have been done actually for several kinds of semicrystalline samples. The result will be reported in the near future.

References and Notes

(1) Tashiro, K.; Wu, G.; Kobayashi, M. *Polymer* **1988**, *29*, 1768.
(2) Kitagawa, T.; Tashiro, K.; Yabuki, K. *J. Polym. Sci., Part B: Polym. Phys.* **2002**, *40*, 1281.
(3) Jungnitz, S.; Jakeways, R.; Ward, I. M. *Polymer* **1986**, *27*, 1651.
(4) Tashiro, K. *Prog. Polym. Sci.*, **1993**, ***18***, 377.
(5) Sakurada, I.; Ito, T.; Nakamae, K. *J. Polym. Sci., Part C* **1966**, *15*, 75.
(6) Brew, B.; Ward, I. W. *Polymer* **1978**, *19*, 1338.
(7) Clements, J.; Jakeways, R.; Ward, I. M. *Polymer* **1978**, *19*, 683.
(8) Brew, B.; Clements, J.; Davies, G. R.; Jakeways, R.; Ward, I. M. *J. Polym. Sci., Part B: Polym. Phys.* **1979**, *17*, 351.
(9) Jungnitz, S.; Jakeways, R.; Ward, I. M.*Polymer* **1988**, *29*, 1768.
(10) Kohlshütter, H. W.; Sprenger, L. *Z. Phys. Chem.* **1932**, *B16*, 284.
(11) Hayashi, K.; Okamura, S. *Makromol. Chem.* **1961**, *47*, 230.
(12) Hayashi, K.; Nishi, M.; Okamura, S. *J. Polym. Sci., Part C* **1963**, *4*, 839.
(13) Enkelmann, V. *Adv. Polym. Sci.* **1984**, *63*, 91.
(14) Wu, G.; Tashiro, K.; Kobayashi, M. *Macromolecules* **1989**, *22*, 188.
(15) Tashiro, K.; Nishimura, H.; Kobayashi, M. *Macromolecules* **1996**, *29*, 8188.
(16) Matsumoto, A.; Matsumura, T.; Aoki, S. *J. Chem. Soc., Chem. Commun*, **1994**, 1389.
(17) Matsumoto, A.; Matsumura, T.; Aoki, S. *Macromolecules*, **1996**, *29*, 423.
(18) Matsumoto, A.; Yokoi, K.; Aoki, S.; Tashiro, K.; Kamae, T.; Kobayashi, M. *Macromolecules*, **1998**, *31*, 2129.
(19) Tashiro, K.; Kamae, T.; Kobayashi, M.; Matsumoto, A.; Yokoi, K.; Aoki, S. *Macromolecules* **1998**, *32*, 2449.
(20) Tashiro, K.; Zadorin, A. N.; Saragai, S.; Kamae, T.; Matsumoto, A.; Yokoi, K.; Aoki, A. *Macromolecules* **1999**, *32*, 7946.
(21) Tashiro, K.; Wu, G.; Kobayashi, M. *J. Polym. Sci.: Part B: Polym. Phys.* **1990**, *28*, 2527.
(22) Tashiro, K.; Minami, S.; Wu, G.; Kobayashi, M. *J. Polym. Sci.: Part B: Polym. Phys.* **1992**, *30*, 1143.
(23) Matsumoto, M.; Katayama, K.; Odani, T.; Oka, K.; Tashiro, K.; Saragai, S.; Nakamoto, S. *Macromolecules* **2000**, *33*, 7786.
(24) Tadokoro, H.; Kobayashi, M.; Yoshidome, H.; Tai, K.; Makino, D. *J. Chem. Phys.* **1968**, *49*, 3359.
(25) Suzuki, M.; Shimanouchi, T. *J. Mol. Spectrosc.* **1969**, *29*, 415.
(26) Nakagawa, I.; Shimanouchi, T. *Spectrochem. Acta* **1962**, *18*, 513.
(27) Shimanouchi, T. *Pure Appl. Chem.* **1963**, *7*, 131.
(28) Iwayanagi, S.; Sakurai, I.; Sakurai, T. Seto, T. *J. Macromol. Sci., Phys.* **1968**, *2*, 163.
(29) Bunn, C. W. *Proc. R. Soc., London* **1942**, *A180*, 40.

MA021090Q